



Revealing new structures in odd–odd ^{54}Mn nucleus

S. Basu^{1,2}, G. Mukherjee^{1,2,a}, S. Nandi^{1,2,12}, S. S. Nayak^{1,2}, S. Bhattacharyya^{1,2}, Soumik Bhattacharya^{1,3}, Shabir Dar^{1,2}, Sneha Das^{1,2}, S. Basak^{1,2}, D. Kumar^{1,2}, D. Paul^{1,2}, K. Banerjee^{1,2}, Pratap Roy^{1,2}, S. Manna^{1,2}, Samir Kundu^{1,2}, T.K. Rana^{1,2}, R. Pandey^{1,2}, S. Chatterjee⁴, R. Raut⁴, S. S. Ghugre⁴, S. Samanta^{4,13}, R. Banik⁵, A. Karmakar^{2,6}, S. Chattopadhyay⁶, S. Das Gupta⁷, P. Pallav^{7,8}, S. Rajbanshi⁹, S. Ali¹⁰, H. Pai^{6,11}

- ¹ Variable Energy Cyclotron Centre, Kolkata 700064, India
² Homi Bhabha National Institute, Training School Complex, Anushaktinagar, Mumbai 400094, India
³ Florida State University, Tallahassee, FL, USA
⁴ UGC-DAE CSR, Kolkata Centre, LB-8, Sector III, Bidhannagar, Kolkata 700106, India
⁵ Institute of Engineering and Management, Saltlake Sector V, Kolkata 700091, India
⁶ Saha Institute of Nuclear Physics, 1/AF Bidhannagar, Kolkata 700064, India
⁷ Victoria Institution (College), Kolkata 700009, India
⁸ Department of Physics, School of Basic and Applied Sciences, Adamas University, Kolkata 700126, India
⁹ Department of Physics, Presidency University, Kolkata 700073, India
¹⁰ Government General Degree College at Pedong, Kalimpong, India
¹¹ Extreme Light Infrastructure - Nuclear Physics, Horia Hulubei National Institute for R&D in Physics and Nuclear Engineering, Bucharest-Magurele 077125, Romania
¹² Present address: Argonne National Laboratory, 9700 S Cass Ave, Lemont, IL 60439, USA
¹³ Present address: University of Genoa, Genoa, Italy

Received: 28 April 2023 / Accepted: 5 October 2023 / Published online: 16 October 2023
© The Author(s), under exclusive licence to Società Italiana di Fisica and Springer-Verlag GmbH Germany, part of Springer Nature 2023
Communicated by Navin Alahari

Abstract The excited states of odd–odd ^{54}Mn ($Z = 25$, $N = 29$) nucleus have been investigated using the fusion evaporation reaction $^{55}\text{Mn}(\alpha, \alpha n)^{54}\text{Mn}$ at the beam energy of 34 MeV. A new and improved level scheme of ^{54}Mn has been proposed in this work with the placement of 22 new γ -ray transitions. Spin and parity (J^π) of most of the levels in the revised level scheme have been firmly assigned. The placement of some of the already known γ rays in the level scheme and J^π assignments of some of the levels reported earlier have also been revised. The new level scheme, which has been extended up to ~ 6 MeV, provides new insight and interesting structural aspects of the generation of high angular momentum in this odd–odd Mn isotope with neutron number ($N = 29$) just above the $N = 28$ shell gap. Three octupole-phonon-coupled negative parity states have been identified for the first time in this nucleus. $E3$ transitions have also been observed to decay from these states. Shell model calculations with two different interactions i.e. kb3gpn and gx1pn have been performed which well reproduced the low-lying, few-particle states but fail to reproduce the higher-lying multi-particle states. These higher-lying states have been understood as resulting from collective excitations. An oblate min-

imum obtained from the Total Routhian Surface calculations provides support to this conjecture.

1 Introduction

The odd–odd ^{54}Mn ($Z = 25$, $N = 29$) is an interesting nucleus from the point of view of nuclear structure. The proton and neutron Fermi energy levels in ^{54}Mn lie below and above the $Z, N = 28$ shell gap, respectively. In fact, the last proton and the last neutron may occupy the $f_{7/2}$ and $f_{5/2}$ orbitals, the $\ell.s$ splitting of which creates the shell gap at 28. This is the first shell gap created due to the $\ell.s$ term which lowers the $1f_{7/2}$ orbital from the rest of the fp space towards the $1d_{3/2}$ orbital [1]. The $N = Z = 28$ nucleus ^{56}Ni is considered as a “soft core” [1,2] compared to the other doubly magic cores in the nuclear chart. For the nuclei in the $A \sim 55$ mass region, the active orbitals are mainly $1f_{7/2}$, $2p_{3/2}$, $1f_{5/2}$ and $2p_{1/2}$. All of these are negative parity orbitals. Therefore, in case of odd–odd nuclei in this region, the excited states are mostly positive parity [3–16]. The negative parity states are mainly observed in the lighter odd–odd nuclei below $A = 50$ [17,18] and only a few negative parity states are known in the nuclei above $A = 50$.

^a e-mail: gopal@vecc.gov.in (corresponding author)

The negative parity states at relatively lower excitation energies reported in the lighter Mn isotopes of $^{52,50}\text{Mn}$ [9, 10], have been interpreted as the result of the coupling of an octupole phonon with the ground state. Consequently, such states have been observed to decay by E3 transitions to the ground state. The 3^- octupole vibration state has also been observed in the even-even ^{52}Fe nucleus [19]. In the previous work, a tentatively assigned negative parity state (7^-) has been assigned to ^{54}Mn by Kiran Kumar et al. [6] at an excitation energy of 1926 keV. However, no E3 transition which can be considered as the evidence of the octupole vibration coupled to the ground state, as in the other odd–odd Mn isotopes, has been observed from this state.

The particle excitation (mostly neutron excitation) to $g_{9/2}$ orbital would also generate negative parity states in odd–odd nuclei in this region. However, this may take place in case of neutron rich isotopes for which the Fermi level is closer to $g_{9/2}$ orbital. In case of lighter nuclei, it needs more energy for excitation to the $g_{9/2}$ orbital. The $g_{9/2}$ orbital is also known for its large shape driving effect. Evidence of the involvement of $\nu g_{9/2}$ orbital has been reported in the neutron-rich isotope of ^{59}Cr ($Z = 24$) [20] nucleus and ^{61}Zn ($Z = 30$) [21] with neutron number $N > 30$. The rotational bands based on $\nu g_{9/2}$ and $\pi g_{9/2}$ have been observed in Cu ($Z = 29$) isotopes also [21]. In case of Mn, the deformed rotational band-like structures have been observed to develop for the neutron rich isotopes of $^{58-60}\text{Mn}$ [4] at the excitation energy of ~ 2 MeV and in ^{56}Mn [3] at ~ 2.5 MeV. These bands have been interpreted as a consequence of neutron occupation in the $g_{9/2}$ orbital, although the spin and parities of the states in these bands are not firmly assigned. In the lighter Mn isotopes, no such band structure based on $g_{9/2}$ configuration has been reported yet. Therefore, the (7^-) negative parity state at a relatively low excitation energy of < 2 MeV in ^{54}Mn , reported in Ref. [6], is some what surprising and needs further investigation.

On the other hand, the $f_{7/2}$ and the $f_{5/2}$ orbitals also show substantial shape driving effects in the Nilsson diagram. Therefore, there has been a quest for identifying deformed states in lighter odd–odd Co and Mn isotopes based on the $\pi f_{7/2}$ and the $\nu f_{5/2}$ configurations [5, 13]. It is worth mentioning that even-even ^{56}Fe ($Z = 26$, $N = 30$) is known to be a deformed nucleus [22, 23] with co-existing prolate and oblate shapes near the ground state. The odd–odd ^{54}Mn has one proton and one neutron less to this shape-coexistent “core” and would be interesting to investigate the effect of the odd particles in stabilizing the core deformation. A band-like structure with a cascade of E2 transitions are reported in the earlier work of ^{54}Mn [6] but the level structure does not seem to form a rotational sequence corresponding to a deformed nucleus.

Therefore, in order to study the excited states in the odd–odd ^{54}Mn nucleus in detail, we have re-investigated its level structure by populating them in a fusion evaporation reaction

using alpha beam and utilizing γ -ray spectroscopy technique. The level scheme of ^{54}Mn has been substantially revised in the present work and new features of the structure of this odd–odd nucleus have been obtained.

2 Experiment and data analysis

The excited states in ^{54}Mn were populated using fusion evaporation reaction $^{55}\text{Mn}(\alpha, \alpha n)^{54}\text{Mn}$ at a beam energy of 34 MeV. The beam was delivered from the K-130 cyclotron at VECC, Kolkata and the prompt γ rays emitted from the de-excited nuclei were detected using an array of 11 Compton-suppressed (CS) clover HPGe detectors and 1 LEPS detector mounted on the upgraded INGA structure at VECC. The target foil, placed at an angle of 55° with respect to the beam direction, was a compound of MnO_2 of thickness ~ 6 mg/cm² on a Mylar backing of 0.5 mg/cm². According to the calculations using PACE-4 (upgraded version of PACE-2, a code for statistical model calculations in heavy ion reactions [24]), four nuclei are mainly populated in the present reaction, these are ^{57}Co , ^{57}Fe and ^{56}Co , in addition to ^{54}Mn . The yield of ^{57}Co was predicted to be maximum with about 40% of the total cross section and the other three nuclei have very similar production cross-sections ($\sim 18\%$ each). The reactions of the beam with the Oxygen in the target and with the Mylar backing were expected to produce Carbon, Nitrogen, Oxygen and Fluorine nuclei with maximum cross section of about 100 mb.

The detectors were placed at three different angles with respect to the beam axis. There were 6 CS clover detectors at 90° , 2 CS-Clovers and the LEPS were at forward (40°) angle and 3 CS-Clovers were at the backward (125°) angle. The two and higher fold coincidence data were collected using a digital data acquisition system. The pulse processing and data acquisition system, based on the 250 MHz, 12-bit PIXIE 16 digitizers (XIA LLC), was that of UGC-DAE CSR, Kolkata Centre [25]. It was found that about 93% of the collected data were two-fold while the rest were three and higher fold.

The data obtained in raw form were processed and sorted in to several symmetric and asymmetric γ - γ matrices and γ - γ - γ cube by the IUCPIX package developed by UGC-DAE-CSR, Kolkata Centre [25]. The energy calibrations of all the crystals of the clover detectors were done for all runs using the standard ^{152}Eu and ^{133}Ba radioactive sources and also using the known in-beam γ lines. For in-beam calibration, γ lines from ^{57}Fe (122.1 keV, 256.0 keV, 1061.6 keV, 1348.9 keV, 1448.5 keV and 1680.6 keV), ^{57}Co (465.7 keV, 1224.0 keV, 1689.4 keV and 2286.0 keV) and ^{56}Fe (846.8 keV, 1238.3 keV and 1303.4 keV) were used. For the calibration of the LEPS detector, ^{133}Ba and some low-energy γ -rays from the ^{152}Eu sources were used. The relative efficiency of the whole array was also determined using the above men-

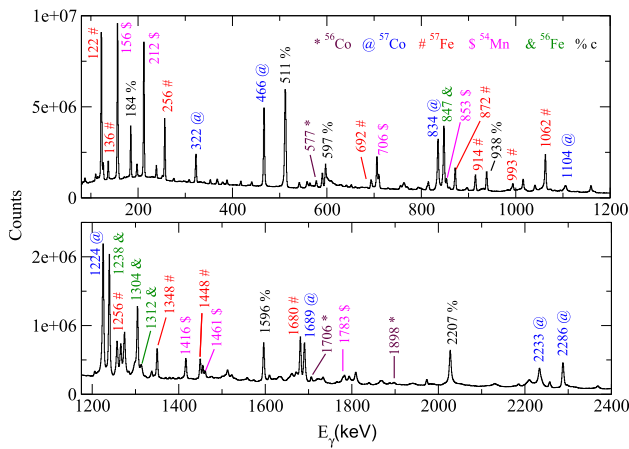


Fig. 1 Total projection spectra from the $\gamma - \gamma$ matrix. The peaks from different nuclei produced in this experiment are identified and labelled in different colours and different symbols. The peaks corresponding to “% c” are from the nuclei which were produced from the reactions of the beam with the Oxygen in the target, the Mylar backing, and possibly very small amount of beam hitting the Aluminium target frame

tioned radioactive sources. Further analysis of the matrices and cube were done using the RADWARE suite of codes [26]. To construct the level scheme, the coincidence and intensity relations of the γ rays were used. The coincidence relation between the γ rays was established using a symmetric $\gamma - \gamma$ matrix, created from the total data with a prompt coincidence window of 200 ns. The $\gamma - \gamma - \gamma$ cube was also used to check the coincidence relations.

A total projection spectrum from the $\gamma - \gamma$ matrix is shown in Fig. 1. It shows some of the peaks from the known γ rays in ^{54}Mn along with those in ^{56}Co , ^{57}Co , ^{57}Fe and ^{56}Fe . It can be seen that the γ -ray peaks from ^{54}Mn are clearly observed with comparable counts to those in ^{57}Fe and ^{57}Co . Two points are worth noting, firstly, we could observe the peaks from ^{56}Fe with reasonable counts that suggests higher production of ^{56}Fe than the PACE-4 prediction of about 4% cross-section. Secondly, the peaks from ^{56}Co (the most intense, lowest lying peaks are marked in the spectrum) could be barely observed with very less counts, though its production cross section was predicted to be similar to those for ^{57}Fe and ^{54}Mn . The other contaminant peaks, marked “%” in the spectrum, were produced from the reactions of the beam with the Mylar backing, the Oxygen in the target and a small fraction of the beam that might have hit the target frame (Aluminium). However, the contaminant peaks are relatively weak and/or of higher energies compared to the most of the primary peaks of interest from the reaction with the Mn target.

The spin and parity assignments of the excited states were done from the measurements of the multipolarity and the polarization asymmetry of the de-exciting γ rays. The multipolarities of the gamma rays were determined from the directional correlation from oriented states ratio (R_{DCO}) [27]. To

measure R_{DCO} , a $\gamma - \gamma$ asymmetric matrix was constructed in which one axis contains the data from the detectors at 125° (θ_1) and other axis from the detectors at 90° (θ_2). Two spectra were generated, gated by the same γ ray on each axis in turn. The intensities of the γ rays of interest were obtained from these two spectra. The values of R_{DCO} of the γ -ray of interest, γ_1 , has been obtained from these intensities using the following relation,

$$R_{DCO} = \frac{I_{\gamma_1} \text{ (measured at } \theta_1; \text{ gated by } \gamma_2 \text{ at } \theta_2)}{I_{\gamma_1} \text{ (measured at } \theta_2; \text{ gated by } \gamma_2 \text{ at } \theta_1)}, \quad (1)$$

where the multipolarity of the gating transition, γ_2 , is known.

The value of $R_{DCO} \sim 1$ corresponds to the same multipolarity of the γ ray of interest as that of the gating transition. However, if the multipolarity of the two transitions are different, then the value of R_{DCO} depends on the mixing ratio of the transition if it is a mixed one, and on the spins of the states. This value also depends on the degree of alignment of the angular momentum of the recoils achieved in the reaction, which is denoted by $\frac{\sigma}{J}$, where σ is the distribution of sub-states centered on $m = 0$ and J is the angular momentum. In case of the alpha-induced reaction as in the present work, we have earlier determined the value of $\frac{\sigma}{J}$ to be ~ 0.37 [28]. We have used this value while calculating the R_{DCO} . The typical value of DCO ratio, calculated for a pure stretched dipole transition gated by a pure stretched quadrupole transition (or vice versa) in our experimental condition is $R_{DCO} \sim 0.7$ (or 1.4).

The electric/magnetic (E/M) nature of the γ rays was assigned from the polarization asymmetry (Δ_{IPDCO}) measurement. The positive (negative) value of Δ_{IPDCO} indicates E(M) type of a γ -ray transition. The polarization (P) of a γ ray can also be obtained as Δ_{IPDCO}/Q , where Q is polarization sensitivity [29]. Clover detectors can act as Compton polarimeter, where the polarization asymmetry can be determined from the difference in the number of perpendicular-scattered γ rays (N_{per}) and parallel-scattered γ rays (N_{par}) using the following relation:

$$\Delta_{IPDCO} = \frac{a(E_\gamma) * N_{per} - N_{par}}{a(E_\gamma) * N_{per} + N_{par}}, \quad (2)$$

where $a(E_\gamma) = N_{par}^u / N_{per}^u$ is the correction factor that is determined from the unpolarized source, where N_{par}^u (N_{per}^u) is the number of parallel (perpendicular) scattered counts of a gamma ray of energy E_γ from the unpolarized source. In order to measure N_{per} and N_{par} , two asymmetric matrices, all vs. N_{per} and all vs. N_{par} , were constructed. Here “all” indicates the data from all the detectors where as, N_{per} and N_{par} indicates the number of counts in the perpendicular and parallel scatterings, respectively, in each of the detectors at 90° . To obtain the gated spectra from these matrices, the gating γ ray peak was selected on the “all” axis and was projected on to the other axis. We have determined $a(E_\gamma)$

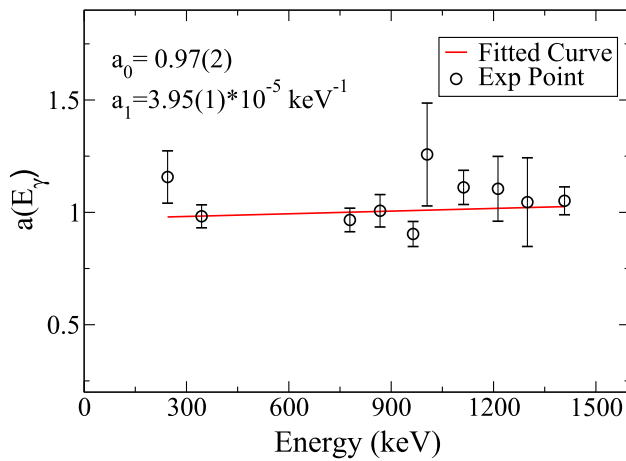


Fig. 2 Asymmetric correction factor, $a(E_\gamma)$, for the detectors at 90° obtained from an unpolarized ^{152}Eu source. Solid line is the linear fit of the experimental data points. The values of coefficients a_0 and a_1 are also given

Table 1 The known E2 transitions in different nuclei, produced in the present experiment, for which $Q(E_\gamma)$ were obtained from the calculated values of polarization (P) and experimentally determined values of Δ_{IPDCO} from our data (see text for details). These $Q(E_\gamma)$ are used in Fig. 3 to deduce the values of the coefficients b_0 and b_1 in Eq. 3

E_γ (keV)	Nuclei	P	Δ_{IPDCO}	$Q(E_\gamma)$
640	^{57}Fe	0.14 (8)	0.03 (9)	0.21 (66)
847	^{56}Fe	0.29 (4)	0.09 (1)	0.31 (6)
993	^{57}Fe	0.31 (2)	0.09 (2)	0.29 (7)
1062	^{57}Fe	0.31 (2)	0.09 (1)	0.29 (4)
1304	^{56}Fe	0.54 (7)	0.09 (2)	0.17 (4)
1416	^{54}Mn	0.61 (10)	0.06 (1)	0.10 (2)
1660	^{57}Fe	1.24 (68)	0.10 (3)	0.08 (5)
2136	^{57}Fe	0.91 (30)	0.05 (6)	0.06 (7)

using ^{152}Eu source, taken after the experiment by putting it exactly at the same position where the target was placed and the aforementioned polarization matrices were constructed from this source data. The ratios of the measured N_{par}^u/N_{per}^u values for different γ -ray energies have been determined and fitted with a linear equation, $a(E_\gamma) = a_0 + a_1 * E_\gamma$. The data and the fitting are shown in Fig. 2. The fitted values of the parameters are obtained as $a_0 = 0.97(2)$, $a_1 = 3.95(1) * 10^{-5} \text{ keV}^{-1}$.

The polarization sensitivity, Q , was also measured experimentally in this work. The polarization sensitivity depends on the energy of the γ rays. Therefore, to measure $Q(E_\gamma)$ we have considered a few strong, known E2 transitions of different energies in different residue nuclei which were produced in our experiment, as shown in Table 1. The polarization (P) of those γ s were calculated following Refs. [29, 30] by taking values of the angular distribution coefficients from the liter-

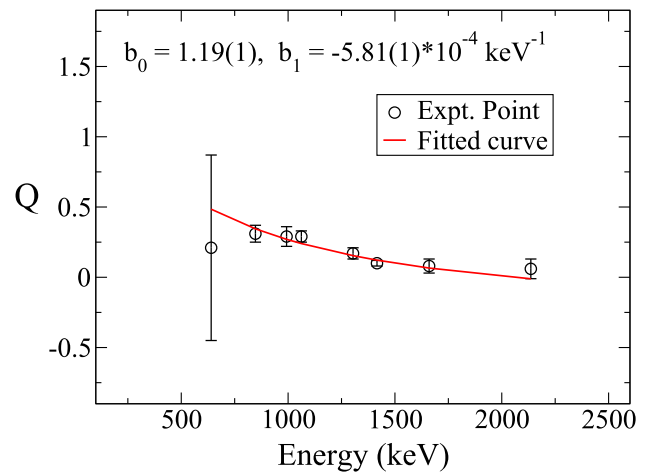


Fig. 3 Experimentally measured Q (Polarization sensitivity) fitted with Eq. (3). The fitted values of the coefficients b_0 and b_1 , are given

ature [7, 22, 31–33]. The $Q(E_\gamma)$ values were then determined for these γ rays from their Δ_{IPDCO} values, measured in this work, and using the relation $Q = \Delta_{IPDCO}/P$, as shown in Fig. 3. These points are fitted using the following equation:

$$Q(E_\gamma) = Q_0(b_0 + b_1 * E_\gamma), \quad (3)$$

$$Q_0 = \frac{1 + \alpha}{1 + \alpha + \alpha^2}, \quad (4)$$

$$\alpha = \frac{E_\gamma}{511}, \quad (5)$$

where, the γ -ray energy E_γ is in keV. The values of the coefficients b_0 and b_1 were obtained from the fit. Usually, the sign (positive/negative) of the measured values of Δ_{IPDCO} are enough to determine the type (E/M) of a gamma transition to assign parity of the levels. However, in the present case, it was necessary to deduce the value of the polarization, P, in order to modify the J^π assignments of some of the levels which are important to understand the structure of ^{54}Mn .

3 Results and discussion

The level scheme of ^{54}Mn , obtained from the present work is shown in Fig. 4. The Table 2 contains information of all the γ rays observed in the present work along with their properties and placement in the level scheme. The energies of the γ rays have been determined from the detectors at 90° . The level energies are determined from the fit to the γ -ray energies.

The level scheme shown in Fig. 4 has been obtained, primarily, by analysing several gated spectra projected from the background-subtracted symmetric matrix. Double-gated spectra projected from the cube were also checked, wherever possible, for confirmation. Sum-gated spectra with gates put on the lowest three intense transitions, i.e 156 keV, 212 keV

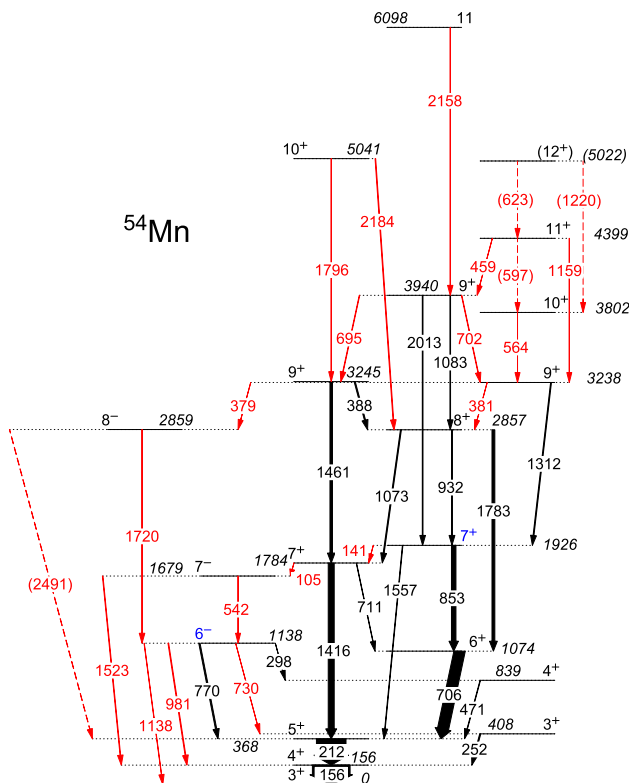


Fig. 4 Newly proposed level scheme of ^{54}Mn . The newly placed or alternately placed γ -rays are shown in red colour. The blue colour indicate different J^π assignment of the level compared to that in Ref. [6]. The width of the arrows are proportional to their intensities. The γ -ray and level energies are rounded off to nearest whole numbers. The dashed transitions are tentatively assigned transitions

and 706 keV are shown in Fig. 5. Most of the known γ rays are observed in this spectrum, along with a few newly observed ones. However, there are a few notable absences as well. The 226-, 349- and 925-keV γ rays, which were reported in the earlier work on ^{54}Mn by Kiran Kumar et al. [6], are not observed in the present work. These unobserved γ rays, along with the 847- and 981-keV ones, were shown in that reference to make a band structure based on a 7^+ state at 1669 keV, which decays to the 6^+ state of the main band by a 596-keV γ ray. We believe that the 847-keV and 596-keV γ rays do not belong to ^{54}Mn with as large intensities as proposed in Ref. [6]. Whereas, we have not found any evidence to the presence of the 847-keV γ ray, we have placed a weak γ ray of 597 keV decaying from the 4399-keV level which is a different location for this transition as compared to that in Ref. [6]. In Ref. [6], the authors showed two spectra with a sum gate (156+212+706 keV), as the one we have shown in Fig. 5, and a spectrum gated by 847-keV γ ray. It may be noted that the 847-keV γ ray is a known $2^+ \rightarrow 0^+$ transition in ^{56}Fe [34]. In the later spectrum of Ref. [6], the relative height of 925-keV peak is about 3-times more than that of 706-keV (a known low-lying intense γ line

in ^{54}Mn), which is in contradiction to their placements in the level scheme shown in Ref. [6]. The remaining γ ray of energy 981 keV has been placed in a different location in our work, decaying from the 1138-keV level to the 156-keV level. This placement is based on the fact that the 981-keV γ ray is observed in the spectrum gated by 156-keV γ ray but not in the spectrum gated by 212-keV γ as can be seen from Figs. 5 and 6. Moreover, the double-gated spectra in Fig. 7, projected from the $\gamma - \gamma - \gamma$ cube, provide further evidence for the placement of the 981-keV transition in the present work. The 981-keV peak is clearly observed in the double gate of 156 keV and 542 keV, but it is absent in the double gate of 212 keV and 542 keV. This placement of the 981-keV transition was also reported in an earlier work on ^{54}Mn [8]. Therefore, the correct placement of 981-keV transition is restored in this work, though the spin and parity of the corresponding level has been newly assigned in our work which has been discussed later.

It might be argued that the γ rays of energy 226 keV, 349 keV and 925 keV, which were not observed in the present work but were observed in Ref. [6], are due to the lack of population of the higher spin states because of the use of α beam for the production of excited states in ^{54}Mn in the present work, compared to the heavy-ion (^{20}Ne) beam, used in the work of Ref. [6]. However, the maximum assigned spin in that work was $15\hbar$ and the PACE-4 calculations show about 60% cross section of the compound nucleus at $15\hbar$ of angular momentum for the reaction in the present work, as shown in Fig. 8. It suggests that the angular momentum population would not be a constraint to observe the decay of the levels which were not observed in the present work.

The placement of 695-keV transition is also changed in the present work, so as to decay from the level at 3940 keV. In the earlier work, it was placed above the 1138-keV level [6]. In Fig. 9, it has been shown that the 695-keV peak is not observed in the spectrum gated by 770 keV but is clearly seen in the spectrum gated by 1073 keV. Moreover, the 695-keV peak is also observed in the spectra gated by 706 keV and 1461 keV transitions as shown in Fig. 10(a) and (c). Therefore, it cannot be placed above 1138 keV level as in Ref. [6]. Two new γ rays, 379 keV and 381 keV, have been observed to decay from the 3238 keV level. They are close in energy but could be identified separately as shown in Fig. 9(a) and (b). The 379-keV peak is observed in the 770-keV gate while 381-keV peak is observed in the spectrum gated by 1073 keV. The placement of these two newly observed γ rays are evident from these coincidence relations. It also confirms the presence of two very close-by energy levels at 2859 keV and at 2857 keV.

The presence of the 702- and 706-keV peaks are also evident from the two gated spectra in Fig. 10(a) and (c). The 706-keV γ was known earlier but the 702-keV γ has been newly placed in the present work. The newly placed 1796-

Table 2 The energy (E_γ) and the relative intensity (I_γ) of the γ rays of ^{54}Mn along with the corresponding spin and parity of the initial (J_i^π) and the final (J_f^π) states and the energy of the initial state (E_i) are shown. The measured values of R_{DCO} and Δ_{IPDCO} of the corresponding γ rays are also given. The uncertainties are given in parenthesis. R_{DCO} values are obtained with a gate on 212-keV pure dipole transition except as noted

E_γ (keV)	E_i (keV)	$J_i^\pi \rightarrow J_f^\pi$	I_γ	R_{DCO}	Δ_{IPDCO}	Assigned multipolarity
104.8 (2)	1784.1 (1)	$7^+ \rightarrow 7^-$	0.26 (2)			E1
141.4 (2)	1925.5 (2)	$7^+ \rightarrow 7^+$	0.25 (3)	1.6 (5)		M1+E2
156.2 (1)	156.2 (1)	$4^+ \rightarrow 3^+$	100 (3)	0.94 (3)		M1+E2
211.9 (1)	368.1 (1)	$5^+ \rightarrow 4^+$	79 (2)	1.04 (3) ¹	-0.06 (1)	M1
251.5 (1)	407.7 (1)	$3^+ \rightarrow 4^+$	2.8 (2)	1.13 (1) ¹	0.01 (3)	M1+E2
298.0 (3)	1137.6 (1)	$6^- \rightarrow 4^+$	0.33 (4)	1.39 (12)	-0.13 (9)	M2
378.9 (7)	3238.1 (2)	$9^+ \rightarrow 8^-$	0.16 (1)	0.94 (12) ²	0.05 (4)	E1
381.2 (3)	3238.1 (2)	$9^+ \rightarrow 8^+$	0.32 (2)	1.25 (8)	-0.09 (9)	M1+E2
388.0 (1)	3245.1 (2)	$9^+ \rightarrow 8^+$	3.0 (2)	0.89 (4)	-0.06 (2)	M1+E2
458.6 (1)	4398.7 (2)	$11^+ \rightarrow 9^+$	0.25 (4)	1.43 (20)	0.23 (17)	E2
471.0 (1)	839.1 (2)	$4^+ \rightarrow 5^+$	1.2 (1)	0.92 (2)	-0.07 (3)	M1+E2
541.6 (2)	1679.1 (2)	$7^- \rightarrow 6^-$	0.44 (6)	0.94 (5)	-0.12 (7)	M1+E2
564.1 (1)	3802.2 (2)	$10^+ \rightarrow 9^+$	0.39 (4)	0.91 (9)	-0.11 (10)	M1+E2
597.0 ⁵	4398.7 (2)	$11^+ \rightarrow 10^+$				M1+E2
622.8 ⁵	(5021.7)	$(12^+) \rightarrow 11^+$	0.04 (2)			M1+E2
695.0 (1)	3940.1 (2)	$9^+ \rightarrow 9^+$	1.29 (15)	1.04 (5) ³	0.07 (7)	M1+E2
702.0 (2)	3940.1 (2)	$9^+ \rightarrow 9^+$	1.15 (11)			M1+E2
705.6 (1)	1073.6 (2)	$6^+ \rightarrow 5^+$	30 (2)	0.82 (2)	-0.05 (1)	M1+E2
710.6 (2)	1784.1 (1)	$7^+ \rightarrow 6^+$	0.85 (11)	0.83 (5) ¹	-0.10 (5)	M1+E2
730.1 (4)	1137.6 (1)	$6^- \rightarrow 3^+$	0.11 (4)	1.41 (10) ¹	0.05 (11)	E3
769.6 (1)	1137.6 (1)	$6^- \rightarrow 5^+$	3.4 (3)	0.98 (1)	0.10 (1)	E1
853.0 (7)	1925.5 (2)	$7^+ \rightarrow 6^+$	12 (1)	0.58 (12) ⁴	-0.06 (4)	M1+E2
931.6 (1)	2857.1 (2)	$8^+ \rightarrow 7^+$	2.3 (2)	0.87 (7) ⁶	-0.01 (1)	M1+E2
981.4 (1)	1137.6 (1)	$6^- \rightarrow 4^+$	1.9 (2)	1.49 (4) ¹	-0.10 (4)	M2
1073.3 (2)	2857.1 (2)	$8^+ \rightarrow 7^+$	2.5 (2)	0.64 (2) ³	0.01 (3)	M1+E2
1083.1 (1)	3940.1 (2)	$9^+ \rightarrow 8^+$	1.57 (13)	0.80 (9) ³	-0.11 (8)	M1+E2
1137.5 (5)	1137.6 (1)	$6^- \rightarrow 3^+$	0.7 (4)			(E3)
1159.0 (8)	4398.7 (2)	$11^+ \rightarrow 9^+$	0.09 (3)			E2
1219.6 ⁵	(5021.7)	$(12^+) \rightarrow 10^+$				E2
1312.4 (4)	3238.1 (2)	$9^+ \rightarrow 7^+$	2.5 (2)	1.52 (21)	0.05 (2)	E2
1416.1 (1)	1784.1 (1)	$7^+ \rightarrow 5^+$	16 (1)	1.30 (7)	0.06 (1)	E2
1460.8 (2)	3245.1 (2)	$9^+ \rightarrow 7^+$	6.7 (5)	0.96 (2) ³	0.07 (1)	E2
1522.6 (2)	1679.1 (2)	$7^- \rightarrow 4^+$	1.5 (2)	1.28 (20) ¹	0.05 (8)	E3
1557.4 (1)	1925.5 (2)	$7^+ \rightarrow 5^+$	1.32 (12)	1.32 (5)	0.14 (8)	E2
1720.1 (9)	2858.6 (6)	$8^- \rightarrow 6^-$	1.6 (2)	1.41 (8)	0.05 (3)	E2
1782.9 (4)	2857.1 (2)	$8^+ \rightarrow 6^+$	7.6 (5)	1.27 (10) ¹	0.06 (2)	E2
1796.2 (7)	5041.1 (5)	$10^+ \rightarrow 9^+$	0.09 (5)	0.66 (8) ³	0.01 (7)	M1+E2
2013.4 (14)	3940.1 (2)	$9^+ \rightarrow 7^+$	1.8 (2)	1.35 (9)	0.14 (10)	E2
2158.1 (8)	6098.3 (8)	$11 \rightarrow 9^+$	0.9 (2)	1.54 (55)		Quadrupole
2183.7 (7)	5041.1 (5)	$10^+ \rightarrow 8^+$	1.7 (2)	1.30 (19)		E2
2490.5 ⁵	2858.6 (6)	$8^- \rightarrow 5^+$	0.2 (1)			(E3)

¹156 keV gate, which is M1+E2 transition with mixing ratio $\delta = -0.03$ [35]

²Pure dipole gate (769.6 keV)

³Pure quadrupole (E2) gate (1416 keV)

⁴Pure quadrupole (E2) gate (1312 keV)

⁵Tentatively assigned transitions

⁶853-keV gate

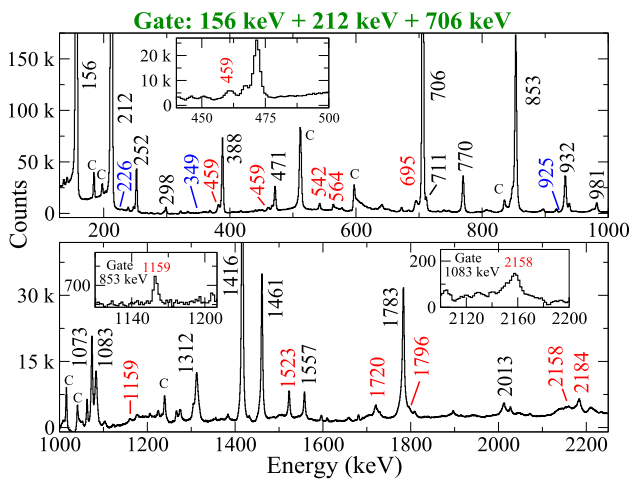


Fig. 5 Sum-gated γ -ray spectrum with gates on the three intense lowest transitions 156 keV, 212 keV and 706 keV of ^{54}Mn . The red-labelled peaks are some of the new γ rays in ^{54}Mn identified in the present work, the blue-labelled numbers correspond to the positions at which “peaks” were reported in Ref. [6] but not observed in our data, the “c” labelled peaks are the known contaminants which belongs either to the other nuclei produced with the ^{55}Mn target (or oxygen present in it) or from target frame (Aluminium). Three new γ -rays have been shown in the insets (in different gates for the 1159 and 2158 keV peaks), which are not clearly seen in the main spectrum

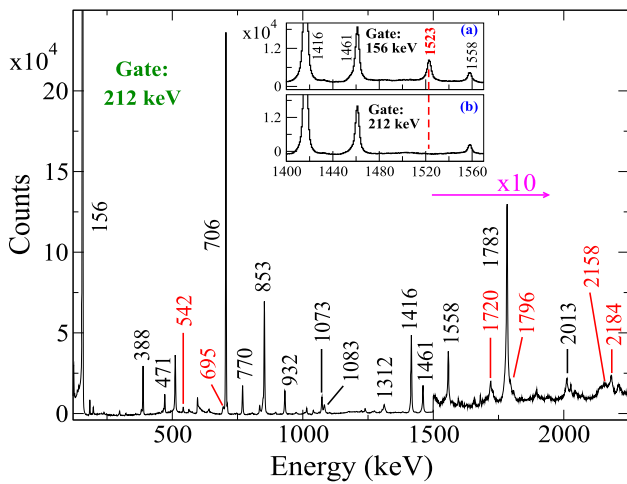


Fig. 6 γ -ray spectrum gated by 212 keV of ^{54}Mn . The new γ rays are labelled in red colour. The presence and absence of 1523-keV transition in 156-keV and 212-keV gated spectra, respectively, are shown in insets (a) and (b)

keV γ ray above the 3245 keV level can be observed in the spectrum gated by 1461 keV but not in the gate of 1083 keV as shown in Fig. 10 (d) and (b), respectively. The known γ -ray of 1783 keV is observed in 1083-keV gate (Fig. 10(b)).

The 542-keV γ line has been newly placed in the level scheme of ^{54}Mn above the 1138-keV level. This γ -ray peak has been identified in the spectra shown in Figs. 5 and 6. A spectrum gated by this 542-keV γ ray is shown in Fig. 11. The known lines of 770 keV and 981 keV are clearly observed

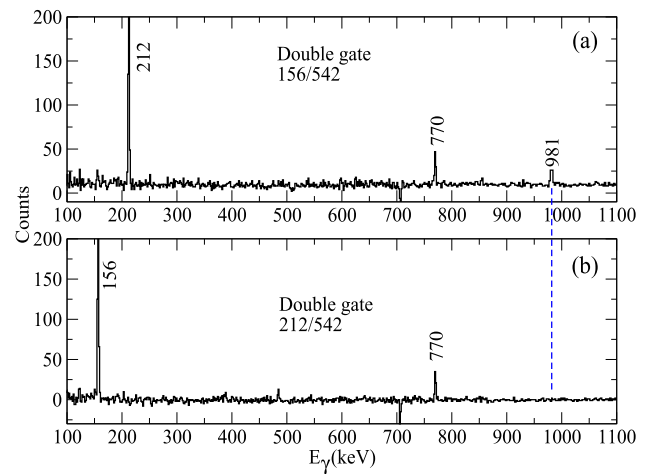


Fig. 7 Double-gated spectra projected from $\gamma - \gamma - \gamma$ cube. (a) Gate on 156 keV and 542 keV γ ray; (b) 212 keV and 542 keV γ ray. The absence of the 981-keV gamma in (b) is shown by the dashed line

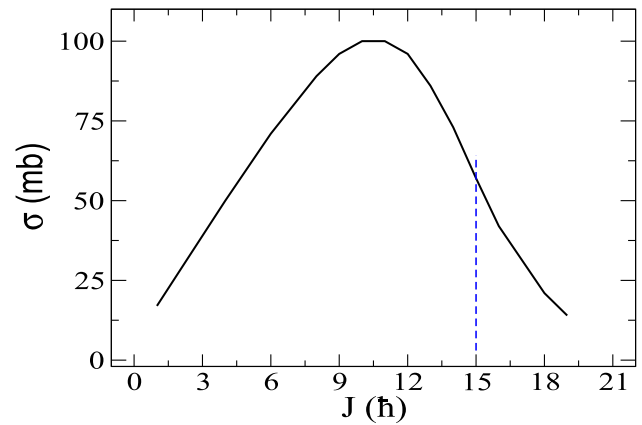


Fig. 8 The population cross-section (σ) in mb as a function of angular momentum (J) in \hbar of the compound nucleus in the reaction $\alpha + ^{55}\text{Mn}$ at 34 MeV as obtained from PACE-4 calculations. It shows about 60% of the maximum cross-section at $J = 15 \hbar$ (dashed line)

in this spectrum, which confirms the placement of the 542-keV line and the 1679-keV level above the 1138-keV level in ^{54}Mn . In addition, the new peaks at 730-keV and 1138-keV are also clearly observed in Fig. 11 and there is clear evidence of the presence of 105-keV and 141-keV peaks (inset (b)) in Fig. 11. These new γ rays can be placed in the level scheme between the known levels in ^{54}Mn . The 730-keV γ ray has been also identified in the spectrum gated by 252 keV as shown in the inset of Fig. 11. Therefore, these two new lines are placed in the level scheme of ^{54}Mn , both of which decay from the 1138-keV level.

A 1523 keV peak can be clearly observed in the sum-gated spectrum in Fig. 5. This peak is also observed in the spectrum gated by 156-keV, $4^+ \rightarrow 3^+$ transition but not observed in the spectrum gated by the $5^+ \rightarrow 4^+$, 212 keV transition as shown in the insets (a) and (b) of Fig. 6. This implies the

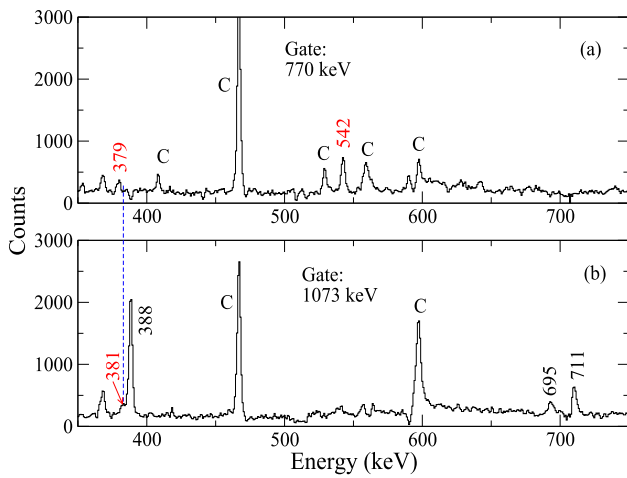


Fig. 9 γ -ray spectra gated by (a) 770 keV and (b) 1073 keV of ^{54}Mn . Newly identified γ s are labelled in red. The peaks labelled as “C” either belong to ^{57}Co , (n,n γ) reaction in the detector material (Ge) or unidentified contaminants

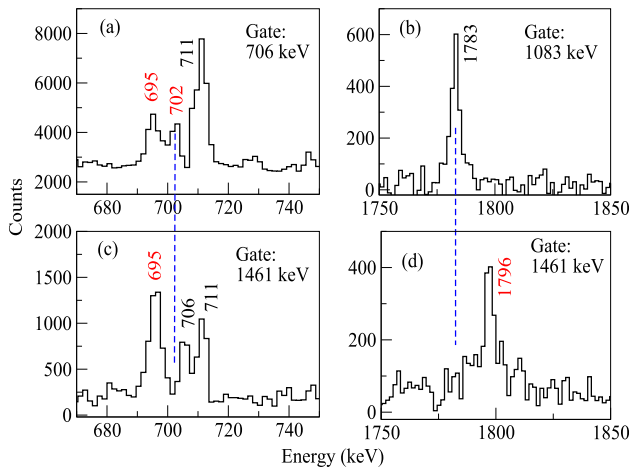


Fig. 10 γ -ray spectra gated by (a) 706 keV, (b) 1083 keV, (c) 1461 keV and (d) 1461 keV transitions of ^{54}Mn . The red-labelled peaks are some of the new γ rays in ^{54}Mn identified in the present work

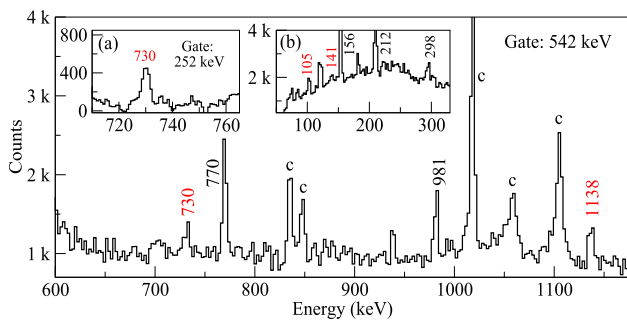


Fig. 11 γ -ray spectrum gated by the 542 keV line showing the newly placed γ -rays 730 keV and 1138 keV, decaying from the 1138-keV level. The 730-keV peak is also clearly observed in the 252-keV gate as shown in inset (a). The inset (b) shows the lower part of the 542-keV gate in which the 105 keV, 141 keV and 298 keV peaks can be observed. The peaks labelled by “c” are either known peaks from other nuclei (primarily from ^{57}Co) or unknown contaminants

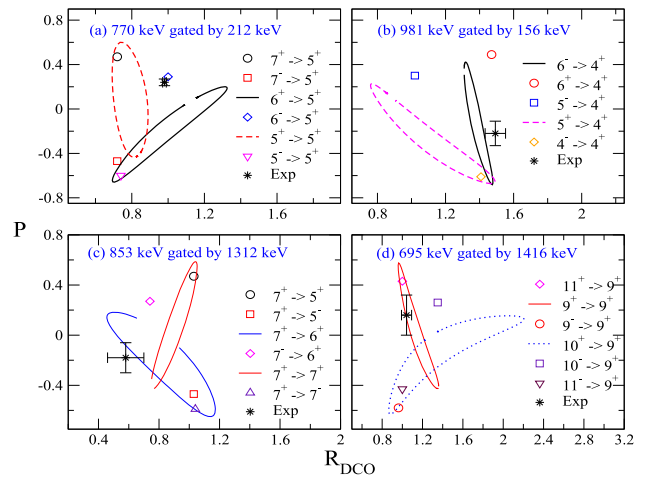


Fig. 12 Plot of measured and calculated values of Polarization (P) vs. DCO ratio (R_{DCO}) for (a) 770-keV (1138 keV–368 keV) transition, (b) 981-keV (1138 keV–156 keV) transition, (c) 853-keV (1926 keV – 1074 keV) transition and (d) 695-keV (3940 keV–3245 keV) transition. The measured values are plotted with a “star” symbol and marked as Exp

presence of the 1523-keV γ -ray from the 7^- state at 1679 keV to the 4^+ state at 156 keV. We have also observed the evidence of the presence of a weak 2491 keV γ ray peak in the gated spectra of both 212-keV and 156-keV. This indicates a possible decay of the 8^- state at 2859 keV to the 5^+ state at 368 keV.

Apart from the new gamma rays and levels, the spin-parity assignments of almost all the levels in ^{54}Mn has been made on the basis of DCO ratio and polarization measurements. The J^π assignments of some of the levels have been modified. Details of a few of the important assignments are discussed below.

The DCO ratio (R_{DCO}) of most of the gamma rays has been measured with a gate on the 212-keV transition which de-excites from the 5^+ state at 368 keV to the 4^+ state at 156 keV. This transition is known to be a $M1$ with very small or no $E2$ admixture [35].

The DCO ratio of the 770-keV γ ray, gated by the 212-keV transition has been found to be close to 1 with a positive value of Δ_{IPDCO} . This suggests an $E1$ assignment for the 770-keV transition and a 6^- assignment for the 1138 keV level. This is in sharp contrast to the 6^+ assignment adopted for this level in [35]. However, this adopted assignment was based on the coincidence angular anisotropy and polarization asymmetry measurement of Ref. [6], the reliability of which measurement is already put in to question. One of the possible reasons for this could be that the excited states in ^{54}Mn were produced in a more complicated reaction of $^{51}\text{V}(^{20}\text{Ne},X)$ at a very high beam energy in that work. We have performed PACE-4 calculation [24] for the above reaction at 145 MeV, which predicted only 5 mb cross-section for

^{54}Mn . The PACE-4 calculation also showed that more than 50 nuclei are produced in that reaction with cross sections similar or more than that for ^{54}Mn . Therefore, the statistics obtained in the spectra shown in Ref. [6] can only be justified if ^{54}Mn was produced in several different types of reactions, e.g. particle transfer, deep inelastic collision, inelastic excitation, evaporation of several particles following fusion, etc., in that measurement. It is quite likely that same pairs of coincident γ rays from more than one nucleus were detected in that experiment. So, clean measurement was not possible in the experiment of Ref. [6]. It is also quite possible that different yrast and non-yrast states of the nucleus of interest were produced in different reaction mechanisms in that case. The angular momentum orientation of the residue is not well known in such cases where different types of reactions are involved. On the other hand, the same PACE-4 calculation for the alpha-induced reaction in the present work shows about 200 mb cross section for ^{54}Mn with only 4 nuclei having similar or slightly more cross-sections, which can be seen in Fig. 1. Therefore, it is expected that other reaction mechanisms mentioned above have not contributed in the present measurement. This is expected also as the energy of the alpha beam was quite low (34 MeV) in the present work.

In order to further investigate, we have determined the value of P of the 770-keV γ ray and compared the measured R_{DCO} and P values with the theoretical calculations for different spins and parities of the 1138-keV state as shown in Fig. 12(a). The calculations are performed with different multipolarities of the transition, such as dipole, quadrupole or a mixed (dipole + quadrupole). For mixed transitions, the calculations are done for different mixing ratios, δ (solid and dashed lines). It can be clearly seen that the experimental values of R_{DCO} and P correspond to a $6^- \rightarrow 5^+$ transition. Similar comparison for the 981-keV transition is also shown in Fig. 12(b). The experimental point for the 981-keV transition is close to the line calculated for $6^- \rightarrow 4^+$, $M2 + E3$ transition for $\delta \sim -0.3$. Therefore, the 981-keV transition is an $M2$ transition with a small ($\sim 10\%$) mixture of $E3$. It may be noted here that the R_{DCO} value for the 981-keV γ could only be obtained with a gate on 156-keV transition, which is a known $M1 + E2$ transition having known mixing ratio $\delta = -0.03$ [35]. From these measurements, a firm assignment of spin and parity of $J^\pi = 6^-$ is made for the 1138-keV level in ^{54}Mn . An additional support for this assignment can also be obtained from the R_{DCO} and Δ_{IPDCO} values of the 298-keV γ ray, decaying from this level to the 839-keV, 4^+ level, which indicates an $M2$ transition (see Table 2). The R_{DCO} and $IPDCO$ ratios could not be determined for the 1138-keV transition. However, since it decays from the newly assigned 6^- state to the 3^+ ground state, an $E3$ assignment of the 1138-keV transition becomes quite obvious. Similarly, the $E3$ nature of the 730-keV γ ray can also be assigned as it decays from this 6^- state to the known 2^{nd}

3^+ state at 408-keV excitation energy. The R_{DCO} value of this transition has been measured as 1.41(10) gated by the 156-keV γ ray. This value is close to the calculated value of ~ 1.47 for an $E3$ transition.

It is worth noting that although the Weisskopf estimate for half-life corresponding to 298-keV, $M2$ transition in ^{54}Mn is about 1 μs , the branching ratio for this transition is less than 6%. On the other hand, the estimated half-life for 981-keV, $M2$ is only about 2.5 ns. Moreover, the branching of the $E3$ transitions i.e., 730 keV and 1138 keV γ rays are also very small. The largest branching ratio is for the $E1$ transition, which is a very fast one. Therefore, the 1138 keV state is not a long-lived isomer despite two $M2$ and two $E3$ transitions decay from it.

The lifetime of this state was measured as 0.88(13) ps by Radford and Poletti [8]. We can compare this lifetime with the Weisskopf estimates of the two most intense transitions of 981 keV $M2$ ($\tau = 2.4$ ns) and 770 keV $E1$ ($\tau = 1.0$ fs). Both the estimated lifetimes become similar (\sim few ns) if it is assumed that the $E1$ transition is hindered by a factor of $\sim 10^6$. However, this underestimates the measured lifetime by a factor of 10^3 . The enhanced $E1$ transition could be a possible reason for this, but it needs further investigation.

A 3220 (20) keV level was assigned $J^\pi = 5^+$ from the angular distribution measurement in ($t, ^3\text{He}$) reaction [36]. This was identified in the ENSDF evaluation [35] as the 3237-keV level reported by Alenius et al. [37]. However, Alenius et al. made tentative spin-parity assignment of $J^\pi = (8,9)$ of this level. Ajzenberg-Selove et al. [36] also associated this level with a 3244 keV level reported earlier. In the present work, the 3238 keV level has been assigned as $J^\pi = 9^+$ from the R_{DCO} and Δ_{IPDCO} values of the 1312 keV γ ray decaying from this state. The $E2$ nature of the 1312 keV transition is quite evident from these values, as shown in Table 2. The newly observed, 381-keV γ ray decaying from this level to the 2857-keV, 8^+ level is found to be of mixed $M1 + E2$ nature from its R_{DCO} and Δ_{IPDCO} values. This provides additional support to the 9^+ assignment of the 3238 keV level. This assignment is in line with that of Alenius et al. [37] but differs from the assignment of [36]. It suggests that the 3220(20) keV level in Ref. [36] is a different level than the 3238 keV level.

There is another 9^+ state at 3245 keV in ^{54}Mn which is very close to the 3238 keV state. These two close-by levels with same spin and parity suggest interaction between them, due to which their energies got perturbed. However, in the present case, we could not determine the interaction strength as the energies of the unperturbed states could not be estimated.

$J^\pi = 7^-$ was assigned to the 1926 keV level by Kiran Kumar et al. [6] from the DCO ratio and polarization asymmetry ratio measurements of the 853-keV γ ray. They have assigned an $E1$ nature of this transition. However, this assign-

ment does not seem to be consistent with the value of DCO ratio (≈ 0.41) that the authors of Ref. [6] had quoted, using a pure dipole gate. We have measured the R_{DCO} of this γ ray with a gate on the 1312-keV, $E2$ transition. We have also determined its P value and compared the measured R_{DCO} and P values with the calculated ones assuming different J^π assignments of the 1926-keV level, as shown in Fig. 12(c). The experimental values clearly indicate a $7^+ \rightarrow 6^+$ transition for the 853-keV γ ray with a mixed, $M1 + E2$ multipolarity. So, we have changed the J^π assignment of the 1926-keV level to 7^+ . The $E2$ nature of the 1557-keV transition (see Table 2) from this level to the 368-keV, 5^+ level further supports this assignment.

The P vs. R_{DCO} plots for the 695-keV transition is shown in Fig. 12(d). The R_{DCO} value in this case is determined with a gate on the 1416-keV, $E2$ transition. The plot clearly shows that the experimental values of P and R_{DCO} match with the calculated values for a $9^+ \rightarrow 9^+$, $M1 + E2$ transition with a mixing ratio of $\delta = 0.75$ (15). Therefore, spin and parity of the 3940-keV level are assigned as $J^\pi = 9^+$. So, the 2013-keV transition from this level to the 1926-keV, 7^+ level has to be an $E2$. The R_{DCO} and Δ_{IPDCO} values of this γ ray (see Table 2) are consistent with a stretched $E2$ transition.

4 Discussion and interpretation of the results

The neutron Fermi level in ^{54}Mn lies above the $N = 28$ shell closure. Therefore, the ground-state J^π of 3^+ in ^{54}Mn is same as that of ^{56}Mn , which is quite different compared to $J^\pi = 6^+$ for the ground state of ^{52}Mn , for which both neutron and proton Fermi levels lie in the $f_{7/2}$ orbitals, below the $N, Z = 28$ shell closure. The low- and medium-energy excited states in ^{54}Mn are explained as 1p3h (1 particle, 3 hole) and 2p4h (intruder) configurations [38]. The 1p3h state at 3245 keV and 2p4h state at 1926 keV were described as “remarkably pure” configurations which primarily decay to the lower-lying 1p3h and 2p4h states, respectively. This is consistent with the 7^+ assignment to the 1926-keV level in the present work. In the present work, we have found that the 1p3h 1784-keV state decays to the 5^+ , 368-keV state with more than 93% branching, indicating a pure 1p3h configuration for this state. However, the branching ratio of about 70%, observed for the decay of the 3245-keV, 1p3h, 9^+ state to the 1784-keV state, indicates a considerable mixing for this state. On the other hand, there are two decay paths from the 2p4h state at 1926 keV to the 1p3h states. One to the 368 keV state by a 1557-keV γ ray and another a newly identified decay path to the 1784 keV state by a weak 141-keV γ ray. This suggests a small mixing of 2p4h and 1p3h configurations for the 1926-keV state, which was previously reported [38] to have a pure 2p4h configuration.

The level scheme of ^{54}Mn has been significantly expanded in the present work. In addition to the known levels in ^{54}Mn , we have identified and placed several new levels in the level scheme of this nucleus. The level scheme has a few interesting features, some of the detailed discussion of the excited states in ^{54}Mn are given below.

4.1 Shell model calculations

The shell model calculations have been attempted for the positive parity states using $fppn$ model space with two different interactions, $gx1pn$ [39,40] and $kb3gpn$ [41] taking ^{48}Ca as core with the code OXBASH [42]. The $fppn$ model space comprises of $1f_{7/2}$, $2p_{3/2}$, $1f_{5/2}$ and $2p_{1/2}$ proton and neutron orbitals. The $\nu 1f_{7/2}$ orbital has always been taken full and all other fp orbitals are free for valence neutrons. The $\pi 1f_{7/2}$ orbital has five protons in the beginning and its excitation to higher fp orbitals are allowed. Therefore, the valence orbitals taken in the configuration space for neutrons are $2p_{3/2}$, $1f_{5/2}$ and $2p_{1/2}$ while for protons, along with the $1f_{7/2}$ orbital, the fp orbitals above $Z = 28$ are also included.

The calculated energies are compared with the experimental ones as shown in Fig. 13. The configuration of the states and the contribution of different neutron orbitals above $N = 28$ for the different excited states in ^{54}Mn are given in Table 3. The configuration of the states are generally given by $\pi(f_{7/2})^5$ and $\nu(f_{7/2})^8(p_{3/2})^{0-1}(f_{5/2})^{0-1}(p_{1/2})^{0-1}$. The contribution of proton orbitals in the fp shell above $Z = 28$ are not given in the Table as their contributions are very small (less than 5%) unless the proton excitations to higher fp orbitals across the $Z = 28$ shell gap are considered (marked as * in Table 3). It is found that the configurations for the yrast states are mostly dominated by $\pi(f_{7/2})^5$ and $\nu(f_{7/2})^8(p_{3/2})^1$ and for the non yrast states $\pi(f_{7/2})^5$ and $\nu(f_{7/2})^8(f_{5/2})^1$.

The percentage contributions of the neutron orbitals obtained from both the interactions are also shown in Fig. 14 for the yrast and the non-yrast states. It can be seen that similar general results are obtained from both the interactions. It is observed that the low-lying yrast states up to $J = 5$ are more pure than the non yrast states. Figure 14 clearly shows that $\nu p_{3/2}$ is the dominant orbital for yrast states and $\nu f_{5/2}$ dominates for the non yrast states.

The Fig. 13 shows that the level energies obtained from the present calculations with both the interactions match well with the experimental ones for almost all the states up to about 3.2 MeV, except for the 6^+ and 7_2^+ states. The states at higher energies, like the non-yrast, 9^+ state observed at 3.9 MeV also could not be reproduced by either of the interactions.

The calculation for the negative parity states required to include $g_{9/2}$ orbital in the configuration space which was outside the scope of the present calculations.

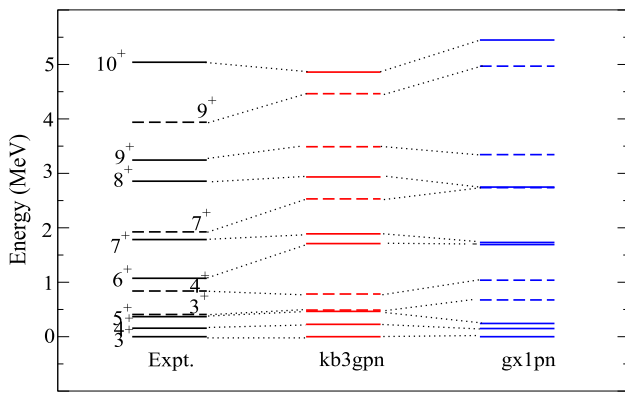


Fig. 13 Comparison of the experimentally obtained states (black) and the shell model calculations with kb3gpn (red) and gx1pn (blue) interactions. The non-yrast states are denoted by dashed lines

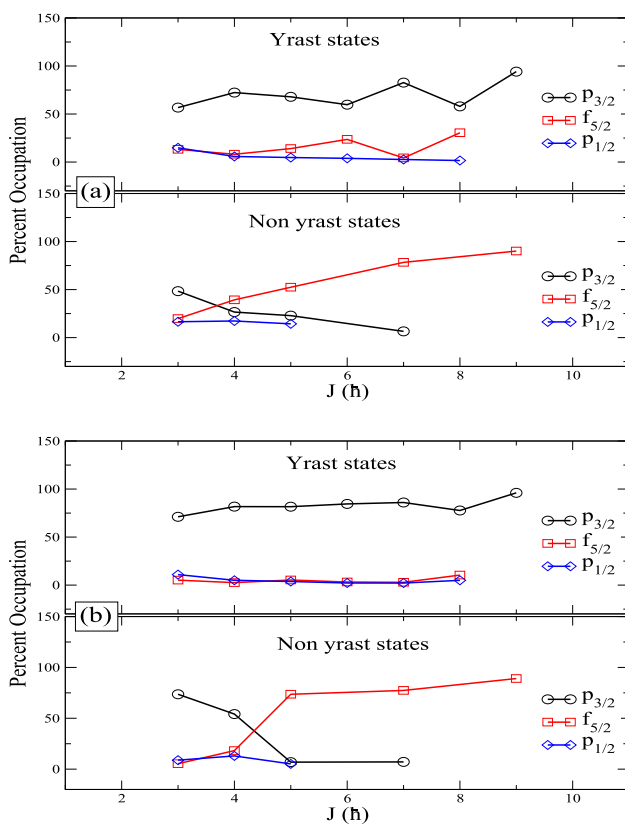


Fig. 14 Calculated percent occupation of valence neutron upper fp orbitals for different angular momentum (J) states using (a) kb3gpn and (b) gx1pn interactions. Different occupation probabilities for the yrast and non-yrast states for a particular J are clearly observed

4.2 The negative parity states

One of the interesting aspects of the present work is the identification of the negative parity states, 6^- , 7^- and 8^- , at 1138 keV, 1679 keV and 2859 keV, respectively, in ^{54}Mn . In case of the lighter nuclei, ^{48}Mn and ^{48}V , the negative parity states

were interpreted as due to the neutron and proton excitation from $d_{3/2}$ to $f_{7/2}$ orbital [17, 18]. Consequently, the lowest negative parity states in these nuclei decay by $E1$ transitions only. However, in case of the negative parity state at 1138 keV in ^{54}Mn , the decay pattern is different. This state has γ -decays to the ground state, two 4^+ states, 5^+ state and to the second 3^+ state. Such negative parity states with $J^\pi = 8^-$ and 9^- have been reported in the neighboring lighter isotopes ^{50}Mn [10] and ^{52}Mn [9], respectively. The J^π of the ground states of these isotopes are 5^+ and 6^+ , respectively. The decay pattern of this negative parity state in ^{54}Mn is very similar to the decay pattern of the other two isotopes, $^{50,52}\text{Mn}$ with $E1$, $M2$ and $E3$ decays, as shown in Ref. [9].

In all the cases, this negative parity state has several decay paths including a $E3$ transition to the ground state. Therefore, the origin of the negative parity state in $^{50,52,54}\text{Mn}$ is different than in ^{48}Mn . The negative parity states in $^{50,52}\text{Mn}$ were interpreted as the coupling of an octupole phonon to the ground state of these nuclei and were compared with the 1^{st} 3^- state in the even-even Fe nucleus. The coupling of this 3^- octupole phonon to the ground state generates the negative parity state in the odd-odd Mn isotopes. Accordingly, the J^π of this octupole state is 8^- , 9^- and 6^- in ^{50}Mn , ^{52}Mn and ^{54}Mn , corresponding to their ground state J^π of 5^+ , 6^+ and 3^+ , respectively. In the case of ^{54}Mn , two distinct features have been observed compared to the other two Mn isotopes. First, the excitation energy of the first octupole-phonon-coupled state is quite low compared to the other two nuclei and secondly, there are two $E3$ transitions from this state, as compared to a single $E3$ transition in the other two isotopes. The excitation energy of the lowest negative parity states in $^{50,52,54}\text{Mn}$ have been shown in Fig. 15 along with the excitation energies of the first 3^- states in the neighboring Fe isotopes. It can be seen that the octupole-phonon-coupled state in odd-odd Mn isotopes follow the systematics of the 3^- states in the neighboring even-even Fe isotopes. It may be noted that for $N > 28$ nuclei, the occupation probability of $g_{9/2}$ increases and so, there will be an enhanced octupole correlation between the $g_{9/2}$ and $p_{3/2}$ orbitals which would lower the energy of this state.

In ^{54}Mn , two more negative parity states, 7^- and 8^- , have been identified in the present work. Both of these states decay to the 6^- state. The 7^- state also has a strong 1523-keV $E3$ transition to the 4^+ state at 156 keV. Similarly, the 8^- state also has a weaker $E3$ decay (2491 keV) to the 5^+ state at 368-keV. These negative parity states could, therefore, be explained as the octupole vibration coupled to the 4^+ and 5^+ states in ^{54}Mn . The observation of octupole vibration coupled states built on the ground state as well as two other excited states is another unique feature in ^{54}Mn for the odd-odd nuclei in this mass region.

Table 3 Shell model calculations showing contribution of different ν fp orbitals using two interactions kb3gpn and gx1pn. The π $f_{(7/2)}$ has 5 particles everytime except those are marked with \star where one or more particle is excited to higher fp orbitals and ν $f_{(7/2)}$ ⁸ is always fixed

Spin (J^π)	Expt	E_x (keV)		Configuration	kb3gpn (contribution in %)	gx1pn (contribution in %)
		kb3gpn	gx1pn			
3 ⁺	0	0	0	p _{3/2}	56.68	71.10
				f _{5/2}	13.20	5.15
				p _{1/2}	14.81	10.95
3 ⁺	408	489	675	p _{3/2}	48.38	73.60
				f _{5/2}	19.77	5.36
				p _{1/2}	16.51	8.83
4 ⁺	156	227	150	p _{3/2}	72.31	81.74
				f _{5/2}	8.08	2.57
				p _{1/2}	5.82	5.02
4 ⁺	839	784	1038	p _{3/2}	26.60	54.15
				f _{5/2}	39.31	18.20
				p _{1/2}	17.30	12.98
5 ⁺	368	465	243	p _{3/2}	67.89	81.63
				f _{5/2}	14.01	5.32
				p _{1/2}	4.68	3.71
6 ⁺	1074	1710	1692	p _{3/2}	59.74	84.49
				f _{5/2}	23.60	3.20
				p _{1/2}	3.86	2.20
7 ⁺	1784	1889	1731	p _{3/2}	86.00	81.63
				f _{5/2}	4.26	2.90
				p _{1/2}	2.67	2.16
7 ⁺	1926	2531	2737	p _{3/2}	6.50	7.11
				f _{5/2}	78.31	77.40
				p _{1/2}		
8 ⁺	2857	2934	2748	p _{3/2}	57.95	77.69
				f _{5/2}	30.45	10.44
				p _{1/2}	1.57	4.96
9 ⁺	3245	3283	3031	p _{3/2}	94.13	96.03
				f _{5/2}		
				p _{1/2}		
9 ⁺	3940	4463	4969	p _{3/2}		
				f _{5/2}	90.08	89.06
				p _{1/2}		
10 ⁺	5041	4860	5449	p _{3/2}		
				f _{5/2}	90.27	91.15
				p _{1/2}		
9 ⁺ \star	3238	7101	6817	p _{3/2}	71.98	91.86
				f _{5/2}		
				p _{1/2}		
10 ⁺ \star	3802	7963	7888	p _{3/2}	86.15	86.62
				f _{5/2}	7.3	8.4
				p _{1/2}		

Table 3 continued

Spin		E_x (keV)		Configuration	kb3gpn	gx1pn
(J^π)	Expt	kb3gpn	gx1pn		(contribution in %)	(contribution in %)
$11^+ \star$	4399	8861	8536	$p_{3/2}$	20.17	97.68
				$f_{5/2}$	72.06	
				$p_{1/2}$		
$11^+ \star$	6098	9104	9197	$p_{3/2}$	78.33	3.51
				$f_{5/2}$	18.59	92.44
				$p_{1/2}$		
$12^+ \star$	5022	9622	9685	$p_{3/2}$	96.33	93.25
				$f_{5/2}$	2.95	3.48
				$p_{1/2}$		

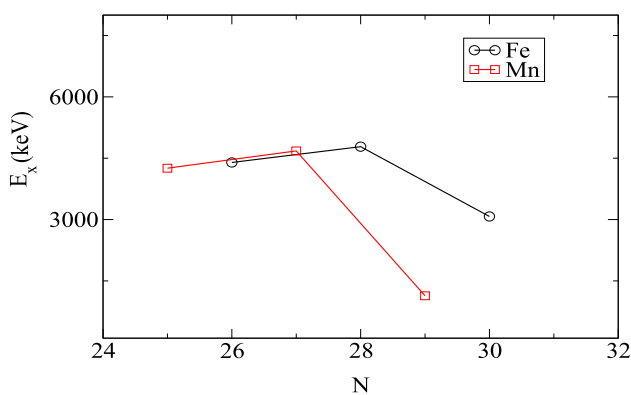


Fig. 15 The excitation energy of the 1st 3^- state in Fe isotopes and energy of the 1st negative parity states in odd-odd Mn isotopes. Both Fe and Mn isotopes are showing similar behaviour, suggesting that the 6^- state in ^{54}Mn is due to the coupling of octupole vibration 3^- to the 3^+ ground state

4.3 Higher spin states and band structure

The $2p4h$, 6^+ and other higher spin states were not well reproduced by the shell model calculations as can be seen in Table 3. These states lie at lower energies than the calculated ones. In case of odd-odd Mn and Co ($Z = 27$) isotopes with neutron number above the $N = 28$ shell gap, band like structures appear, which indicates the onset of deformation. In ^{56}Mn , Nathan et al., observed a regular level structure above 2.2 MeV which resembles a rotational band [3]. However, the spin and parities of the states could not be determined. Similarly, in ^{58}Mn and ^{60}Mn , the shell model calculations were able to reproduce only the low-lying states, mostly below 1.5 MeV excitation [4]. Clear rotational band-like structures have been observed in these heavier odd-odd Mn isotopes above the states with tentatively assigned spin of $7\hbar$. The spin and parities of the possible collective states could not be assigned in these nuclei. The involvement of $\nu g_{9/2}$ was

conjectured for the onset of collectivity at higher excitation energies in these nuclei.

In case of ^{54}Mn rotation-like structure, similar to the heavier isotopes of Mn seems to have developed above the 8^+ state at 2857 keV through the 564 keV–597 keV–623 keV sequence of transitions. The plot of excitation energy (E_x) vs. spin (I) for the three Mn isotopes ($^{54,56,58}\text{Mn}$) are shown in Fig. 16 for which the neutron Fermi levels lie above $N = 28$ shell gap. The rotational model formula ($E_x = A_0 + A_1 * I(I + 1)$, where A_0 and A_1 are the parameters) fits the data points well for all the three isotopes. It was noted earlier that, the $2p4h$, 6^+ and 7^+ states at 1074 and 1926 keV match well with the shell model calculations but calculations start to deviate from the 2857-keV 8^+ state. It can be seen from the level scheme in Fig. 4 that another set of levels, corresponding to a different configuration, starts to build up on top of the 8^+ state. This is clearly seen from the E_x vs. I plot in the inset of Fig. 16 where, the lower spin part is also shown along with the higher spin part. The rotational model fits are equally good for both the regions with different slopes and the high spin part has a larger moment of inertia than the lower part. This clearly suggests that the higher spin part corresponds to a configuration which involves more numbers of unpaired nucleons. It may be noted that the E_x vs. I plot for the lower spin part in the $N = 29$ isotones ^{54}Mn and ^{56}Co are very similar, indicating an onset of deformed configuration at $N = 29$ for these nuclei with neutron Fermi level above the $N = 28$ shell gap.

4.4 TRS calculation

In order to further investigate the possible deformed structure in ^{54}Mn , the Total Routhian Surface (TRS) calculations have been performed in the microscopic-macroscopic approach. The Nilsson-Strutinsky formalism has been employed with Woods-Saxon potential for these calculations [43,44]. The detailed technical procedure has been given in Refs. [45–

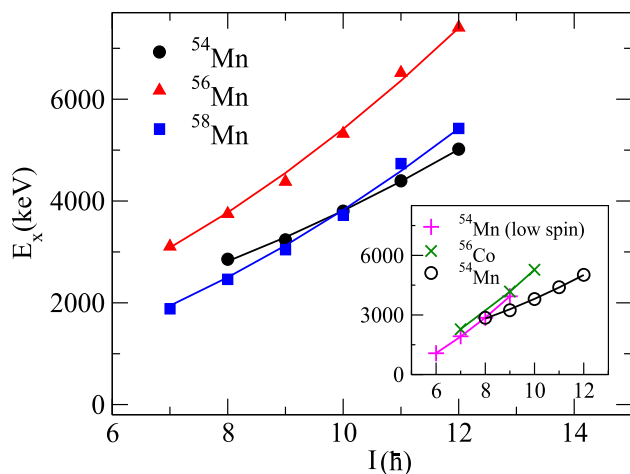


Fig. 16 Excitation energy (E_x) vs. spin (I) plot for the three Mn isotopes ($^{54,56,58}\text{Mn}$) for which neutron Fermi level is above $N = 28$ shell gap. The same plots for the lower spin parts in the $N = 29$ isotones ^{54}Mn and ^{56}Co are shown in the inset. Data for ^{56}Mn , ^{58}Mn and ^{56}Co are taken from Refs. [3–5], respectively. The solid lines are the fits to the rotational model formula in both the plots

47]. The total Routhian energies, calculated in the $(\beta_2, \gamma, \beta_4)$ mesh points, are plotted in the $\beta_2 - \gamma$ plane as contour plots, following minimization on β_4 . The Lund convention is followed in these calculation in which, $\gamma = 0^\circ$ corresponds to a collective prolate and $\gamma = -60^\circ$ corresponds to a collective oblate shape. The calculations are done for different quasi-particle configurations. The β_2 and γ values at the minimum in the contour plots for a particular configuration correspond to the deformation of the nucleus.

The contour plots of the TRS, calculated for the 2p4h configuration, are shown in Fig. 17. A well defined minimum is obtained in the TRS plot with deformation parameters $\beta_2 = 0.27$ and $\gamma = -68^\circ$. This indicates a collective oblate shape for ^{54}Mn for the multi-particle configuration. This is consistent with the rotational band-like structure observed in the present work.

5 Conclusion

The medium to high spin states in the odd–odd nucleus ^{54}Mn have been investigated by populating them in the alpha-induced fusion evaporation reaction of $^{55}\text{Mn}(^4\text{He}, \alpha n)^{54}\text{Mn}$. The γ -ray spectroscopy technique with an array of 11 clover detectors was used for this. A new and improved level scheme has been obtained. In particular, the level scheme presented in Ref. [6] has been substantially modified in the present work. This modified level scheme provides a new understanding on the structure of odd–odd ^{54}Mn nucleus.

Most of the low-lying states, up to around 3 MeV of excitation energy, could be reproduced well in the shell model

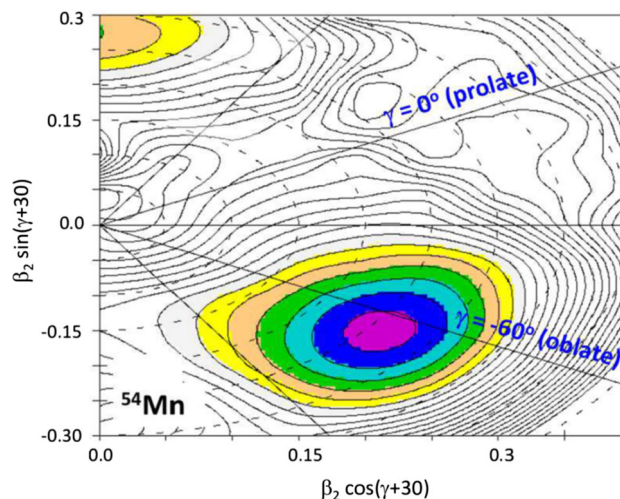


Fig. 17 Contour plots of the TRS calculations performed for ^{54}Mn at rotational frequency $\hbar\omega = 0.561$ MeV. A well defined minimum at oblate deformation ($\gamma \sim -60^\circ$) is obtained in the calculation. The contours are 250 keV apart

calculations, performed with two interactions. However, the higher-lying states could not be reproduced well.

With the firm spin-parity assignment and identification of new γ decays, the 6^- state in this nucleus has been identified as originating from the coupling of octupole phonon with the ground state. The excitation energy of this octupole vibrational state has been found to be at a much lower excitation energy compared to the lighter odd–odd Mn isotopes, but in agreement with the systematics of the 3^- states in the neighboring Fe isotopes. Two more negative parity states were also identified at higher excitation energies which were also explained as the coupling of octupole phonon with the excited 4^+ and 5^+ states. However, we could not extend much the negative parity states to observe any state involving $\nu g_{9/2}$ orbital.

An onset of deformation for the higher-lying, multi-particle states has been proposed from the observation of rotational band-like structure and comparison with the other neighboring nuclei with neutron Fermi level above $N = 28$ shell gap. An oblate minimum obtained from the TRS calculations supports this onset of deformation in ^{54}Mn .

In this region with neutron number above $N = 28$ shell closure, the occupation of $g_{9/2}$ orbital induces large deformation in the system. It would be interesting to extend the negative parity states in ^{54}Mn in a future experiment to look for the negative parity rotational band structure to identify the shape-driving effect of the $g_{9/2}$ orbital.

Acknowledgements The authors thank the operators and support staff of the K-130 Cyclotron at VECC, Kolkata for providing good quality α beam and all the collaborators involved in this campaign for setting up the detector array. The tremendous help and support of Dr. Dirtha Sanyal (VECC) and the target lab staff of VECC are gratefully acknowledged

for lending the material and preparation of the MnO_2 target for the experiment. S. Basu, S. Dar and S. Basak acknowledge the financial support of UGC, Govt. of India. S. Das and A. Karmakar acknowledge CSIR, Govt. of India for their financial support.

Data Availability Statement This manuscript has no associated data or the data will not be deposited. [Authors' comment: Data generated for the study of this nucleus are contained in this published article.]

References

1. K. Arnsward et al., Phys. Lett. B **820**, 136592 (2021)
2. T. Otsuka, M. Honma, T. Mizusaki, Phys. Rev. Lett. **81**, 1588 (1998)
3. A.M. Nathan et al., Phys. Rev. C **16**, 192 (1977)
4. D. Steppenbeck et al., Phys. Rev. C **81**, 014305 (2010)
5. M. Palacz et al., Nucl. Phys. A **627**, 162 (1997)
6. G. Kiran Kumar et al., J. Phys. G: Nucl. Part. Phys. **35**, 095104 (2008)
7. M. Toulemonde et al., J. Phys. G: Nucl. Part. Phys. **5**, 6 (1979)
8. D.C. Radford, A.R. Poletti, J. Phys. G: Nucl. Phys. **5**, 3 (1979)
9. M. Axiotis et al., Phys. Rev. C **76**, 014303 (2007)
10. C.E. Svensson et al., Phys. Rev. C **58**, R2621 (1998)
11. A. Giorni et al., Nucl. Phys. A **292**, 213 (1977)
12. S.A. Milne et al., Phys. Rev. Lett. **117**, 082502 (2016)
13. D. Rudolph et al., Phys. Rev. C **82**, 054309 (2010)
14. M.A.G. Silveira et al., Phys. Rev. C **74**, 064312 (2006)
15. D. Rudolph et al., Phys. Rev. Lett. **80**, 3018 (1998)
16. C.D. O'Leary et al., Phys. Lett. B **525**, 49 (2002)
17. F. Brandolini et al., Phys. Rev. C **66**, 024304 (2002)
18. M.A. Bentley et al., Phys. Rev. Lett. **97**, 132501 (2006)
19. C.A. Ur et al., Phys. Rev. C **58**, 6 (1998)
20. S.J. Freeman et al., Phys. Rev. C **69**, 064301 (2004)
21. O. Izotova et al., Phys. Rev. C **69**, 037303 (2004)
22. N. Bendjaballah et al., Phys. Rev. Lett. **36**, 1536 (1976)
23. D.E. Appelbe et al., Phys. Rev. C **62**, 064314 (2000)
24. A. Gavron, Phys. Rev. C **21**, 230 (1980)
25. S. Das et al., Nucl. Inst. Meth. Phys. Res. **A893**, 138 (2018)
26. D.C. Radford, Nucl. Instrum. Methods Phys. Res. A **361**, 297 (1995)
27. A. Kramer-Flecken et al., Nucl. Instrum. Methods Phys. Res. **A275**, 333 (1989)
28. S. Nandi et al., Phys. Rev. C **99**, 054312 (2019)
29. R. Palit, H.C. Jain, P.K. Joshi, S. Nagaraj, B.V.T. Rao, S.S. Chintalpuudi, S.S. Ghugre, PRAMANA-J. Phys. **54**, 347 (2000)
30. S. Rajbanshi et al., Phys. Rev. C **89**, 014315 (2014)
31. A.M. Nathan et al., Phys. Rev. C **17**, 3 (1978)
32. P. Banerjee et al., Nuovo Cim. **85A**, 54 (1985)
33. D.G. Sarantites et al., Phys. Rev. C **14**, 4 (1976)
34. H. Junde, S. Huo, Y. Dong, Nucl. Data Sheets **112**, 1513 (2011)
35. Y. Dong, H. Junde, Nucl. Data Sheets **121**, 1 (2014)
36. F. Ajzenberg-Selove, Ronald E. Brown, E. R. Flynn, J. W. Sunier, Phys. Rev. C **32**, 756 (1985)
37. L.G. Alenius et al., Nuovo Cimento **27**, 249 (1975)
38. J.P. Johnstone et al., J. Phys. G: Nucl. Part. Phys. **3**, L69 (1977)
39. M. Honma, T. Otsuka, B.A. Brown, T. Mizusaki, Phys. Rev. C **65**, 061301 (2002)
40. M. Honma, T. Otsuka, B. Brown, T. Mizusaki, Eur. Phys. J. A **25**, 499 (2005)
41. A. Poves, J. Sánchez-Solano, E. Caurier, F. Nowacki, Nucl. Phys. A **694**, 157 (2001)
42. Oxbash for Windows, B. A. Brown et al., MSU-NSCL report number 1289 (2004)
43. W. Nazarewicz, J. Dudek, R. Bengtsson, T. Bengtsson, Nucl. Phys. A **435**, 397 (1985)
44. W. Nazarewicz, M.A. Riley, J.D. Garrett, Nucl. Phys. A **512**, 61 (1990)
45. G. Mukherjee et al., Nucl. Phys. A **829**, 137 (2009)
46. S. Samiran Nayak, G. Mukherjee, Nucl. Phys. A **1023**, 122449 (2022)
47. S. Samiran Nayak, G. Mukherjee, Int. Jour. Mod. Phys. E **31**, 2250048 (2022)

Springer Nature or its licensor (e.g. a society or other partner) holds exclusive rights to this article under a publishing agreement with the author(s) or other rightsholder(s); author self-archiving of the accepted manuscript version of this article is solely governed by the terms of such publishing agreement and applicable law.